Unsaturated biobased polyesters from bicyclic α-pinene-based diols

Research Article

Received: 14 November 2025 Revised: 17 March 2026 Published online in Wiley Online Library:

(wileyonlinelibrary.com) DOI 10.1002/pi.70127

Unsaturated biobased polyesters from bicyclic α-pinene-based diols

Ganapathy Ranjani,[a,b†] Shengwei Sun,[a,b†] Erik Sundén,[a,b] Diana Bernin[c] and Per-Olof Syrén[a,b*]

Abstract

Here we report the synthesis and characterization of a set of four unsaturated prepolymers made from polycondensation of two (−)-α-pinene-derived bulky diols, *trans*-hydroxy nopol (HN) and *trans*-hydroxy myrtenol (HM), with dimethyl itaconate and dimethyl maleate as renewable acyl donors. Structure verification by ^{1}H and ^{13}C NMR in concert with Fourier transform infrared analyses confirmed intact backbone C=C groups and ester formation in these prepolymers, showing number-average molar masses between 1.4 and 6.3 kg mol^{-1} and dispersity in the range 1.3–2.2. The intact pinene core concomitant with the chiral arms protruding from it results in elevated thermal stability, manifested by 5% weight-loss temperatures (T_5) above 220 °C and decomposition maxima reaching 315 °C, concomitant with an elevated glass transition temperature for one of the materials (T_g of 45 °C). Finally, to investigate end-of-life options, subjecting the four polymers to depolymerization studies using the leaf-branch compost cutinase resulted in partial depolymerization for the less flexible maleate-containing polyesters, liberating the corresponding diol monomers (8% HN and 13.5% HM). Biodegradation was further supported by shifted SEC traces toward lower molar mass. Complementary *in silico* docking and metadynamics studies were used to identify near-attack conformations in which the ester carbonyl in the *cis*-alkene-containing, maleate-based bulky backbones is ready for hydrolysis. Overall, this study highlights the untapped potential to generate biobased unsaturated polyesters by capitalizing on rigid bicyclic terpene-based diols, resulting in elevated thermal performance while retaining enzymatic degradability.

Supporting information may be found in the online version of this article.

Keywords: biobased polymers; enzymatic hydrolysis; terpenes; unsaturated polyesters

INTRODUCTION

Since synthetic polymers and plastics were industrialized almost a hundred years ago,[1] their production has been skyrocketing and is expected to reach 600 million tons year^{-1} within the next few decades.[2] In 2020 the plastic production globally amounted to *ca* 550 million tons, with the bulk originating from fossil-based virgin monomers.[3] Today, only *ca* 14% of synthetic plastics can be made from closed- and open-loop recycling schemes.[3] The immense potential of using biomass-derived building blocks[3] to generate biobased polymers[4,5] was recognized early, but still only *ca* 2% of all synthetic polymers are currently biosourced.[6] The environmental and socioeconomic burden attached to the currently implemented plastics economy leads to the release of significant amounts of greenhouse gases, corresponding to 5% of the total industrial emissions, pollution and the generation of microplastic particles that affect ecosystems and possibly human health.[7–9] Significant efforts to curb these consequences associated with current manufacturing and mismanagement of synthetic polymers are under way.[10–20]

A key component of a future circular plastics economy[12] is the generation of biosourced[21–23] synthetic polymers that are recyclable.[6] In particular, replacing petroleum-based polyesters that have a market share of *ca* 60 million tons year^{-1} with biobased alternatives is in the spotlight. Their hydrolyzable ester bond (bond-dissociation energy *ca* 100 kcal mol^{-1} [24,25]) facilitates depolymerization at end-of-life and renders polyesters potentially biodegradable.[26] Challenges in the generation of biobased polyesters include the necessity of oxidative functionalization[27] of biomass-derived building blocks to activate them for polymerization[28] and the need for replicating the strength and thermal properties of fossil-based plastics.[29,30] Suitable properties for engineering applications often require high thermal stability

* *Correspondence to: P-O Syrén, School of Chemistry, Biotechnology and Health, Science for Life Laboratory, KTH Royal Institute of Technology, Tomtebodavägen 23 171 65, Solna, Sweden, E-mail: per-olof.syren@biotech.kth.se (Syrén)*

† *These authors contributed equally to this work.*

a *School of Chemistry, Biotechnology and Health, Science for Life Laboratory, KTH Royal Institute of Technology, Solna, Sweden*

b *School of Engineering Sciences in Chemistry, Biotechnology and Health, Department of Fibre and Polymer Technology, KTH Royal Institute of Technology, Stockholm, Sweden*

c *Department of Chemistry and Chemical Engineering, Chalmers University of Technology, Gothenburg, Sweden*

and elevated glass transition temperatures, which can be a challenge to achieve particularly when starting from aliphatics from biomass. For instance, the atactic form of the prominent bioplastic poly(lactide) is amorphous, calling for stereoselective polymerization routes to enable materials with higher performance, such as heat resistance induced by tacticity and optimized packing interactions in the polymer chain.[31–34]

Besides (hemi)celluloses and lignin, terpenes have emerged as a potent source of biobased building blocks for material science, including polyester, polycarbonate, polyamide and polyurethane formations.[28,35–51] Terpenes constitute the most diverse family of natural products with more than 100 000 structures known from all kingdoms of life.[52] Terpenes are often multicyclic scaffolds harboring stereocenters formed via the underpinning stereoselective enzymatic carbocationic cyclization cascades. If the ring structure and chirality of multicyclic terpenes can be preserved during functionalization and polymerization, strong aliphatic materials can be attained due to the rigidity of the terpene cyclic core. Further augmentation of interchain interactions is achieved by the chiral substituents protruding from the repeating unit, resulting in attractive mechanical properties in the responding polymer.[38] Still, to make terpenes compatible with polyester formation often necessitates the installation of additional hydroxyl and/or cyclic ester groups onto the cyclic core.[28] We previously reported the first generation of (−)-α-pinene-derived polyesters via chemoenzymatic upcycling into verbanone lactone, which was prone to undergo ring-opening polymerization[51] resulting in polyesters with a pendant cyclobutyl motif in the backbone. In contrast to the first generation pinene-based polyesters that had a low molecular weight (<3 kg mol^{-1}), the second generation[49] pinene-derived polyesters were instead generated by polycondensation from the diol 1-(1′-hydroxyethyl)-3-(2′-hydroxy-ethyl)-2,2-dimethylcyclobutane (HHDC) generated by oxidative cleavage of the (−)-α-pinene ring and which resulted in increased molecular weight (8 kg mol^{-1}). More recently, we directly functionalized (−)-α-pinene so that the hydroxyls were directly attached to the bicyclic core.[53] Co-polymerization of these pinene-based diols with methyl esters of aliphatic and aromatic renewable diacids resulted in polyesters harboring an intact bicyclic pinene ring and with tunable T_g and high thermal stability (above 260 °C).

In comparison with saturated terpene-based polyesters, their unsaturated counterparts have received much less attention (Fig. 1(a)).[38] Unsaturated polyesters have found key applications in coatings, adhesives and composites.[54] The C=C double bond provides reactive handles for post-functionalization by click chemistry, including thiol-ene based transformations.[55] The utilization of terpene scaffolds for providing the unsaturated part has up to now involved transacylation of the monoterpenol sobrerol[50,56] to its methacrylated form (Fig. 1(a), top left), embedding an unsaturated isoprenyl in poly(dihydrocarvide) stemming from the ring-opening polymerization of monoterpenoids[57] or in polycarbonate formation from limonene oxide.[58] Co-polymerization of diesters of maleate, fumarate or itaconate with the α-pinene-derived diol (HHDC) to give UV-curable polymers (Fig. 1(a), bottom) has been disclosed.[49] Unsaturated terpene-based polyesters with backbones of increasing steric bulk were obtained by myrcene–itaconate cycloadducts, resulting in photocurable polyester formulations[59] (Fig. 1(a), right). Finally, the sesquiterpene β-elemene has been embedded in polyester materials (Fig. 1(a), top).

Building on these trends, we herein explore the possibility of introducing a bicyclic terpene core in the backbone of unsaturated biobased polyesters (Fig. 1(b)). To this end, we capitalized on two (−)-α-pinene-derived chiral diols, *trans*-hydroxy nopol (HN) and *trans*-hydroxy myrtenol (HM), recently reported by us.[53] Polycondensation with dimethyl itaconate (DMI) and dimethyl maleate (DMM) resulted in prepolymers with either exo-methylene or maleate (*cis*-alkene) unsaturation, and their effect on chain growth and the properties of the resulting prepolymers (molar mass, T_g) was analyzed. Finally, enzymatic depolymerization for two of the materials could be achieved by leaf-branch cutinase (LCC). This study illustrates how bicyclic terpene diols can confer high performance and end-of-life options.

MATERIALS AND METHODS

Chemicals and reagents

(1*R*)-(−)-nopol (98%), (1*R*)-(−)-myrtenal (98%), (1*R*)-(−)-myrtenol (95%), borane-THF (1.0 mol L^{-1} in tetrahydrofuran, THF), 2-MeTHF (anhydrous), H_2O_2 (30% in H_2O), sodium hydroxide (97%), DMI (98%) and DMM (99%) were purchased from Sigma-Aldrich, Sweden. Ethyl acetate (ACS, Reag. Ph. Eur.), dichloromethane, chloroform, methanol, ethanol, *n*-heptane and magnesium sulfate were obtained from VWR Chemicals, and xylene (analytical grade, ACS) from Scharlau, Spain. All other solvents and reagents were purchased from Sigma-Aldrich, Sweden unless otherwise specified.

Synthesis of monomers and polyesters

General procedure

Pinene-based diols were synthesized as previously described by diastereoselective hydroboration followed by the oxidation sequence from myrtenol and nopol, respectively.[53] The diol monomer (HN (1) or HM (2)) (1.00 equiv.), a diester (DMI (3) or DMM (4)) (1.0 equiv.), dibutyltin oxide (DBTO) (2 mol% of the corresponding diol monomer) and mequinol (0.5 wt% of the total monomer) were added to a three-necked round-bottom flask equipped with a mechanical stirrer. The reaction mixture was heated to 120 °C for about 10 min under a flow of N_2 and stirred at this temperature until the completion of transesterification (approximately after 3 h, as observed by ^{1}H NMR). Afterwards, the flow of N_2 was increased, and the mixture was heated to 140 °C and stirred at this temperature until the completion of polymerization. Then, the reaction mixture was transferred to a Teflon Petri dish, with a small amount of $CHCl_3$ being used to transfer the material left in the reaction flask. The Petri dish was covered with aluminium foil, and the solvent was evaporated at room temperature and dried under vacuum at 25 °C for 24 h, yielding the corresponding polyester. The unsaturated polyesters synthesized from monomer HN (1) and dimethyl itaconate and fumarate were denoted HN_DMI (5) and HN_DMM (6), respectively. Similarly, the polymers obtained from monomer HM (2) were denoted HM_DMI (7) and HM_DMM (8).

For the polyesters (7), (8) obtained from the monomer (2), 1 mL of xylene was added during the transesterification step and refluxed due to the sublimation of the HM monomer. The polyesters obtained from the monomer HN (1) were synthesized under solvent-free conditions. Once the reaction was completed, the reaction mixture was transferred to a molten state and dried under vacuum at room temperature. Drying at higher than room temperature or removing the inhibitor by purifying with

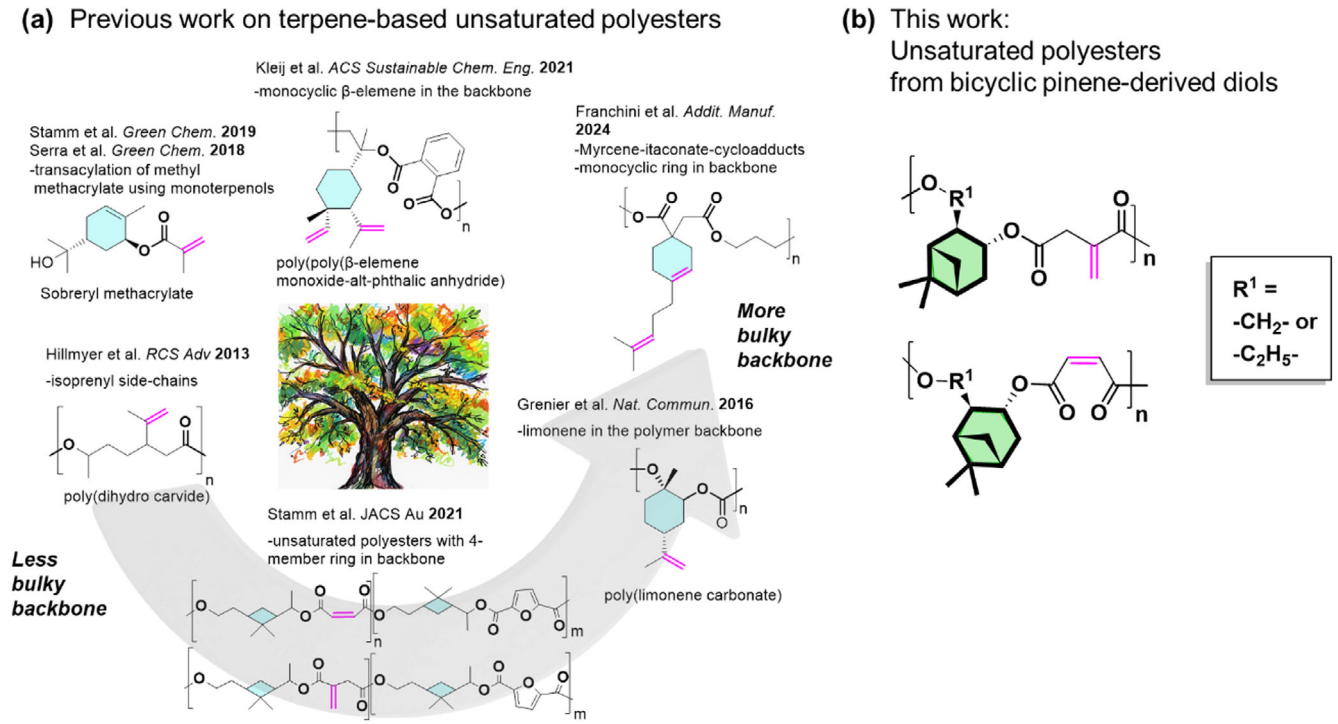

Figure 1. Previous (a) and present (b) work on polyesters from terpene-based diols. Unsaturation is highlighted in magenta, monocyclic terpene rings in cyan, and the bicyclic pinene core explored herein in green.

methanol resulted in crosslinking of the polyesters. Hence the crude polyesters were taken for the analysis.

Characterization of polyesters

Nuclear magnetic resonance spectroscopy

^{1}H and ^{13}C NMR spectra were recorded on a Bruker Avance 400 spectrometer at 298 K. Chemical shifts (δ) are reported in ppm relative to $CDCl_3$. The operating frequencies were 400.13 MHz for ^{1}H and 100.61 MHz for ^{13}C.

Attenuated total reflectance Fourier transform infrared spectroscopy

Fourier transform infrared (FTIR) spectra were recorded on a PerkinElmer 2000 spectrophotometer equipped with an attenuated total reflection accessory. Each sample was scanned eight times over the range 400–4000 cm^{-1}.

Size exclusion chromatography

The molecular weights of the polyesters were determined by SEC. SEC elugrams were recorded on a Malvern GPCMAX system equipped with a PLgel 5 µm guard column (7.5 × 50 mm) and two PLgel 5 µm MIXED-D analytical columns (300 × 7.5 mm) maintained at 35 °C. Number-average molecular weights (M_n) and dispersity ($Đ$) values were calculated relative to a calibration curve obtained with narrow-dispersity polystyrene standards (370–364 000 g mol^{-1}). The eluent was HPLC-grade $CHCl_3$ containing 2% (v/v) toluene. Polyesters were dissolved in the eluent and allowed to stand for 12 h before filtration through a 0.22 µm membrane filter. A 100 µL aliquot of each sample solution was then injected for analysis.

Thermogravimetric analysis

TGA was conducted on a Mettler Toledo TGA 1 instrument at a heating rate of 10 °C min^{-1} under a nitrogen atmosphere with a purge rate of 50 mL min^{-1} over the temperature range 50–600 °C, and the thermal decomposition maxima (T_d), 5% weight loss (T_5) and char yield were determined. TGA data were processed using Mettler Toledo STARe v. 15.00 software.

Differential scanning calorimetry

DSC measurements were performed using a Mettler Toledo DSC 1 instrument at a heating rate of 10 °C min^{-1} under a nitrogen flow rate of 50 mL min^{-1}. The temperature program consisted of a heating ramp from −30 to 200 °C, followed by a cooling ramp to 0 °C, and finally a second heating ramp to 200 °C. The glass transition temperature (T_g) was determined from the second heating cycle. Data were analyzed using Mettler Toledo STARe v. 15.00 software.

Enzyme production and purification

The plasmids carrying the LCC gene were transformed into the chemically competent *Escherichia coli* CD43(DE3) cells using the heat-shock method. The transformants were then inoculated into 5 mL 2 × yeast extract tryptone (YT) medium containing 50 µg mL^{-1} ampicillin, and incubated at 37 °C with 180 rpm shaking overnight. The following day, 1 mL of the overnight culture was inoculated into 100 mL of fresh 2 × YT medium supplemented with the same concentration of antibiotic. The cultures were incubated at 37 °C for 2–3 h until the optical density at 600 nm reached 0.6–0.8, after which protein production was induced by the addition of 1 mmol L^{-1} isopropyl β-D-1-thiogalactopyranoside (IPTG). After cells were incubated at 18 °C for 24 h, the cell pellets were harvested using centrifugation at 4000*g* and 4 °C for 10 min.

Polymer International published by John Wiley & Sons Ltd on behalf of Society of Chemical Industry.

They were then resuspended in 25 mL Tris–HCl buffer (25 mmol L^{-1}, pH 7.5) and lysed using sonication on a Branson SFX 250 instrument (45% power, 2 s pulse and 4 s off) on ice. The cell lysates containing crude enzymes were clarified by centrifugation at 4000*g* for 20 min. The ÄKTA explorer™ protein purification system (GE Healthcare, IL, USA) equipped with 1 mL HisTrap HP prepacked columns (Cytiva, Amersham, UK) was used to purify the enzymes. Proteins were eluted using a gradient of imidazole concentration from 0% to 100%. Desalting was performed with PD-10 columns (Cytiva, Amersham, UK) against an equilibration buffer of 25 mmol L^{-1} Tris–HCl (pH 7.5), following the manufacturer's instructions. Protein concentrations were determined using a NanoDrop spectrophotometer (VWR, PA, USA), and purity was assessed by sodium dodecyl sulfate polyacrylamide gel electrophoresis (SDS-PAGE).

Enzymatic degradation of polymers

10 mg of each polymer (5)–(8) (HN_DMI, HN_DMM, HM_DMI and HM_DMM) were weighed and then incubated with 20 µg purified enzyme in 1 mL Tris–HCl buffer solution (25 mmol L^{-1}, pH 7.5) at 50 °C and 800 rpm for 24 h. After reaction, these reaction buffers were freeze-dried for 48 h. Polymer samples incubated without any addition of enzymes were used as a control group. Finally, all dried samples were re-dissolved in $CDCl_3$ or HPLC grade $CHCl_3$ containing 2% (v/v) toluene for NMR and SEC analysis, respectively.

Computational methods

Docking was conducted in AutoDock Vina 1.2.5[60] using Dockey[61] 1.0.3 as a graphical user interface. Molecular dynamics (MD) was run using OPENMM[62] 8.2.0 with topologies prepared using OpenFF-Toolkit 0.15.2, and PDBFixer 1.9. Amber ff14SB[63] was used as a protein force field, while Sage 2.2.1[64] with AM1-BCC charges was used to parameterize small molecules representing the repeating unit. Water and ions were parameterized using tip3pfb.[65] A time-step of 4 fs was used together with a pressure of 1 bar and a temperature of 300 K. Well-tempered metadynamics were run using the same software suite as for standard MD.[66] Bonds were biased with 0.5 Å Gaussians with a height of 1 kJ mol^{-1} deposited every 500 steps with a bias factor of 4. Simulations were analyzed using MDAnalysis[67,68] 2.8.0, mdaencore[69] 1.0.0 and ProLIF.[70] Structures were visualized in ChimeraX[71] 1.9. The setup, running and analysis of MD is automated in our in-house package WhatCat to allow for the entire MD workflow to happen with one command-line input (https://github.com/Erikna00/WhatCat). For any additional details on the setup of the MD simulations, we refer the reader to WhatCat's source code.

Binding pose generation

To produce a surrogate holo-structure, the model substrates were docked into the most suitable crystal structure, PDB ID 7VVE,[72] possessing a 2 Å resolution along with a substrate analog bound in the active site with good electron density overlap between the assigned and calculated structure. ChimeraX with the Dunbrack rotamer library was used to revert the S165A mutation present in the literature structure, introduced to allow for crystallization with ligand.

The docked poses closest to the oxyanion hole (5–6 Å from Met166 amide proton) were selected for 1D Metadynamics (MTD). The collective variable was chosen to be the distance between the backbone amide proton in Met166 and the closest of the carbonyl oxygens in the substrate. A single replicate of 200 ns was run for each selected pose with the intention to use accelerated sampling to locate open active site conformations. This was successful with clusters containing near attack conformations (NACs) found for each of the two substrates. Poses where the catalytic triad hydrogen bond network was preserved and the distance between oxyanion hole and substrate carbonyl oxygen was below 3 Å were extracted and used for a second round of docking to try to find more favorable binding poses. This was successful, yielding one good pose per substrate. These poses, referred to as the manual poses, were used for the production MD, which was run for 200 ns in triplicate.

A separate avenue to try to produce bound poses using the structure prediction software Boltz-2[73] was also explored. To do this Boltz-2 was run using the sequence extracted from PDB ID 7VVE and the smiles of each substrate, utilizing physical potentials and a pocket restraint on S165 and Met166 set to a maximum distance of 3.5 Å but with force equaling False. Five poses per substrate were produced.

These were distinct from those produced manually, but did, however, suffer from Boltz-2 not respecting the sp^2 nature of a carbonyl carbon and the conjugation of the carbonyl to adjacent alkene, necessitating further refinement. Therefore, promising poses were subjected to 100 ns MTD using the same collective variable as in the manual curation. Poses with the substrate carbonyl closer than 3 Å to the oxyanion hole were retained, referred to as the Boltz poses and used for production MD. We would have liked to only use poses with an intact catalytic triad hydrogen bond network, but no snapshot fulfilled this requirement.

RESULTS

Synthesis and characterization of unsaturated terpene-based polyesters harboring a bicyclic core

The chiral (–)-α-pinene-derived diols HN (1) and HM (2) were copolymerized with DMI (3) and DMM (4) to obtain a set of four unsaturated pinene-based polyesters (5)–(8) (Scheme 1).

The structures of the polyesters were confirmed by ^1H and ^{13}C NMR spectroscopy. Figures 2 and 3 show the comparison of ^1H NMR spectra of the polyesters (5)–(8) with those of the corresponding monomers HN (1) and HM (2). During polymerization, new ester peaks appeared in the four polymers (arrows in Figs 2 and 3), stemming from a shift of the proton adjacent to the secondary hydroxyl. Signals from $–OCH_3$ end groups are also clearly visible in the spectra (boxes, Figs 2 and 3). The methylene groups in the diesters were found intact, confirming that the materials are not crosslinked under the reaction conditions (peaks with a shift above 5.5 ppm). Further, the structures of the polyesters were confirmed by ^{13}C spectroscopy (see the Supporting Information). Multiple peaks appeared in the ^{13}C spectra of the polyesters, which are due to the presence of two different hydroxy groups (1°–OH and 2°–OH) and different ester groups in the itaconate unit. A complex peak multiplicity was also observed due to rotamer formation in HM_DMM (8).

All the polyesters (5)–(8) were further characterized by FTIR analysis (Figs 4(a), 4(b)). The –OH observed at *ca* 3320 cm^{-1} for the diol monomers (HN (1), HM (2)) disappeared in the polymers. A new peak was observed at *ca* 1715–1735 cm^{-1}, which corresponds to the ester carbonyl stretching signal. C–H stretching for saturated and unsaturated carbons was observed around *ca* 3000 cm^{-1}. Ester –C–O stretching was observed at *ca* 1130 cm^{-1}, alkene C=C stretching was observed at 1642 cm^{-1}, $–CH_2$ wagging was observed at around 950 cm^{-1}

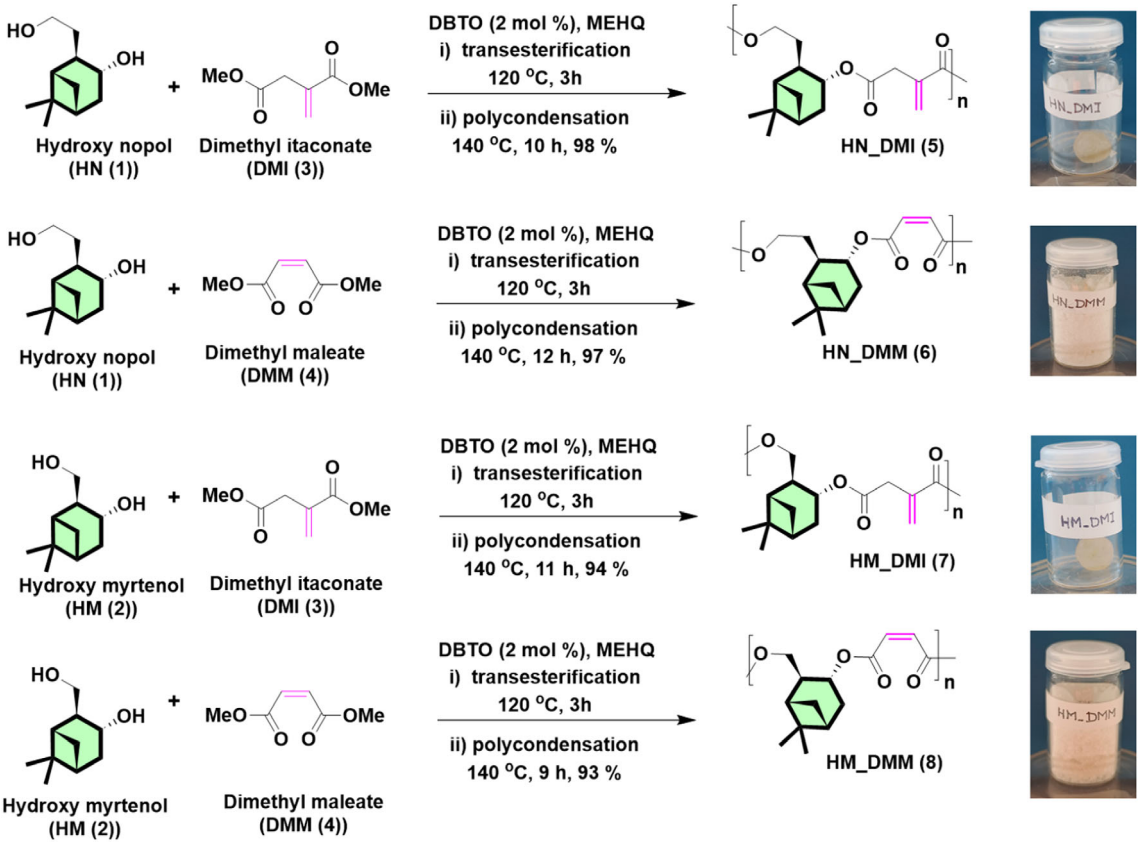

Scheme 1. Synthesis of unsaturated polyesters (5)–(8), conditions 2 mol% of DBTO catalyst and mequinol (MEHQ) (0.5 wt% of the total monomer) as radical inhibitor. Once the transesterification was finished, the polycondensations were conducted at 140 °C to afford the unsaturated polyesters HN_DMI (5), HN_DMM (6), HM_DMI (7), HM_DMM (8), respectively.

and the remaining peaks in the polymers (5)–(8) match with those of the monomers. The number- and weight-average molar mass (M_n and M_w) and dispersity ($Đ$) of the polyesters (5)–(8) measured from SEC, as shown in Fig. 4(c), are presented in Table 1. The molar mass found from SEC is low (around 2 kg mol^{-1}), as the samples are not purified after polymerization, which is also reflected by a higher value of dispersity index (Table 1). The dispersity of the polyesters (5)–(8) is in the range 1.3–2.2. Although M_n from SEC is slightly lower than those theoretically calculated from NMR (Table 1), both are overall well in agreement with each other. The thermal stability of the polyesters (5)–(8) evaluated by TGA and DSC, shown in Figs 4(d), 4(e), is summarized in Table 1. All the polyesters showed a thermal decomposition above *ca* 220 °C (T_5, measured at 5% weight loss), and they are thermally more stable than the monomers (1), (2). In addition, the observed char yield for the polyesters was *ca* 0%–20% (Figs 4(d), 4(e), Table 1). Thermal transitions of the polyesters (5)–(8) were evaluated by DSC and are shown in Figs 4(d), 4(e) and summarized in Table 1. T_g of the HN_DMI (5) and HM_DMI (7) are almost identical (15, 13 °C) while that of the HM_DMM (8) is higher than that of the HN_DMM (6). Polyesters from the respective diol monomer and DMM (6), (8) have shown higher T_g than those made by co-polymerization using DMI (5), (7) (Figs 4(d), 4(e), Table 1).

Enzymatic depolymerization of the unsaturated polyesters

LCC is well known to degrade various polyesters such as poly(ethylene terephthalate) (PET), poly(trimethylene terephthalate) and poly(butylene terephthalate).[74] This bioprocess involves the hydrolysis of ester bonds, breaking down the polymers into their monomer components. In our previous studies, we also found that LCC exhibited significant degradation activity toward bulky terpene-derived polyesters.[53,75] NMR and SEC analyses confirmed that it cleaved the ester bonds, releasing the corresponding monomers. For these reasons, here we employ LCC as a potential biocatalyst to depolymerize the newly synthesized unsaturated prepolymers, including HN_DMI (5), HN_DMM (6), HM_DMI (7) and HM_DMM (8). Following enzymatic reactions, we did not observe apparent changes in the ^{1}H NMR spectra for the itaconate-containing polymers HN_DMI (5) and HM_DMI (7), while the disappearance and formation of new peaks were identified in the ^{1}H NMR spectra for the maleate-based materials HN_DMM (6) and HM_DMM (8) (Figs 5(a), 5(b)). Peaks appearing at *ca* 3.6 ppm and 2.5 ppm in the NMR spectra of the polyester after enzymatic degradation (labeled HN_DMM_LCC) correspond to the monomer HN peaks (Fig. 5(a)); peaks showing at *ca* 3.6 ppm and, to a lesser extent, 2 ppm in the spectra of HM_DMM_LCC following enzymatic degradation correspond to the monomer HM peaks (Fig. 5(b)). Estimation of the yield by peak integration demonstrated that the enzyme LCC produced 8% HN and 13.5% HM monomer, respectively. These results suggest that the LCC can hydrolyze the polyesters by breaking down the ester bonds. We also confirmed enzymatic depolymerization of the maleate-based polyesters HN_DMM and HM_DMM using SEC

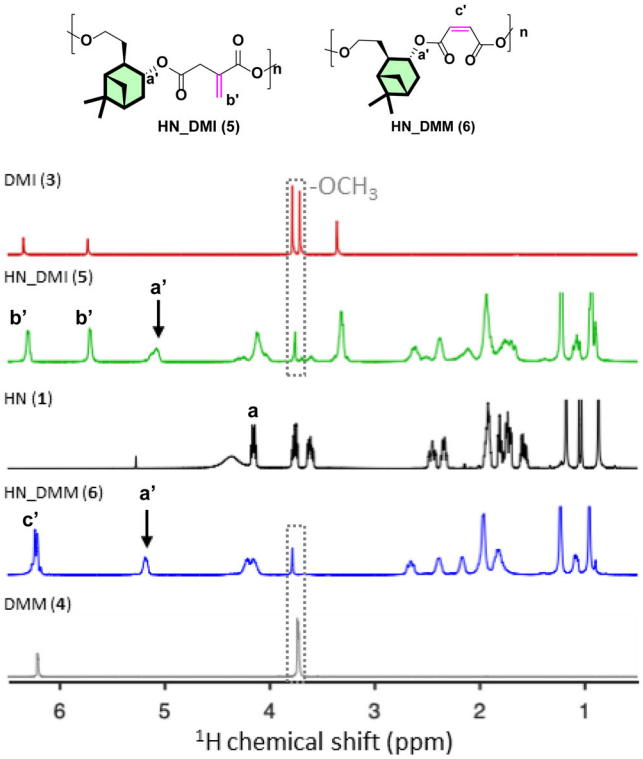

Figure 2. ^{1}H NMR analysis of HN-based materials. Comparison of ^{1}H NMR spectra of the polyesters HN_DMI (5), HN_DMM (6) with those of the monomer HN (1), DMI (3) and DMM (4). The –OCH_3 end groups are shown in the boxes and the arrows indicate the formation of ester.

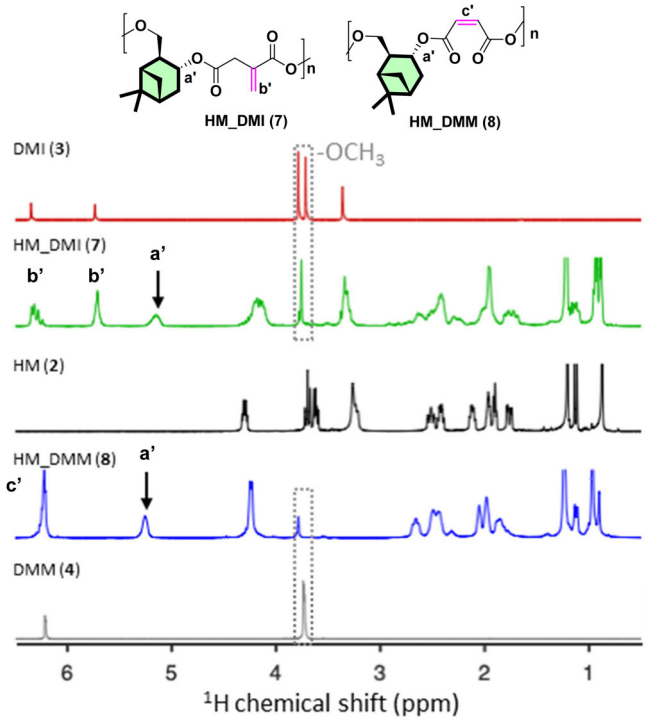

Figure 3. ^{1}H NMR analysis of HM-based materials. Comparison of ^{1}H NMR spectra of the polyesters HM_DMI (7), HM_DMM (8) with those of the monomer HM (2), DMI (3), DMM (4). The –OCH_3 end groups are highlighted in the boxes, and the formation of the ester is indicated with the arrows.

analysis. The results showed a slight decrease in the number-average molecular weight (M_n), accompanied by a shift of the polymer peak toward higher retention volumes. In addition, two new peaks appeared in the SEC profile, indicating that degradation occurred during enzymatic incubation (Figs 6(a), 6(b)). Next, we used docking and MD to understand the degradation mechanism based on these findings.

Study of the geometry of the enzyme–substrate complex by binding pose generation and MD

We have elucidated that LCC prefers twisted chains (i.e. *gauche* conformations), both in the degradation of PET[76] (Fig. 7(a)) and for saturated biobased polymers.[38] Therefore we were interested in how the unsaturated polymers that were experimentally confirmed to be degradable would interact with the active site (Fig. 7(b)).

To explore the degradation of HN_DMM (6) and HM_DMM (8) we wanted to look at NACs of the model substrates into the active site of LCC. However, after inspecting the available crystal structures, no suitable holo-structure for our bulky substrates was found, as judged by the steric congestion around the catalytic triad (S165-H242-D210) and accompanying oxyanion hole. Hence, bound poses were generated (Figs 8(a), 8(b)) as described in Materials and Methods to yield a manual pose and a Boltz-2 pose for each model substrate. These were subjected to 200 ns of MD in triplicate.

Analyzing the MD trajectories for all poses showed that the model substrates, which are forced into bent conformations due to the *cis* alkene, further bind to LCC exclusively with the carbonyls in the *gauche* conformation, similar to LCC's preferred binding pose with PET[76] (shown in Fig. 7(a)). Moving on, analyzing the trajectories with ProLIF revealed that the key binding interaction of the substrate is the hydrophobic interaction between one of the terpene subunits and the hydrophobic cleft formed by Y95, M166 and W190, which will henceforth be referred to as the 'eastern pocket' (see Supporting Information). This interaction was never broken in any replicate in any of the MD trajectories after it had been sampled. The binding interactions in the western pocket, however (referring to the pocket formed by G94, T96, A97, S101, H164, I243, N246; see Supporting Information), were much less preserved over the trajectories, probably due to the lower hydrophobicity of this western pocket and the inability of our substrate to form hydrogen bonds to T96 and N246 due to the orientation of the methoxy group. The model substrate HM2_DMM bound well and stayed in the manually prepared NAC for the entire trajectory in all triplicates. The Boltz pose performed worse, shifting to a binding mode where one of the carbonyl oxygens, instead of pointing towards the oxyanion hole, was now hydrogen bonded to S165 and Y95, producing a non-reactive conformation which was stable for the rest of the simulations.

HN2_DMM in the manually prepared NAC bound for around 15 ns before shifting into hydrogen bonding with S165 and Y95 in approximately the same non-reactive conformation as the Boltz pose of HM2_DMM. One of the replicates also showed a complete dissociation out of the western pocket, with the entire substrate binding now occurring between V215, F125 and the eastern pocket. The Boltz pose of HN2_DMM stayed bound in the prepared pose for around 25 ns, but the hydrogen bond to M131 to complete the oxyanion hole was only formed in a minority of

Polymer International published by John Wiley & Sons Ltd on behalf of Society of Chemical Industry.

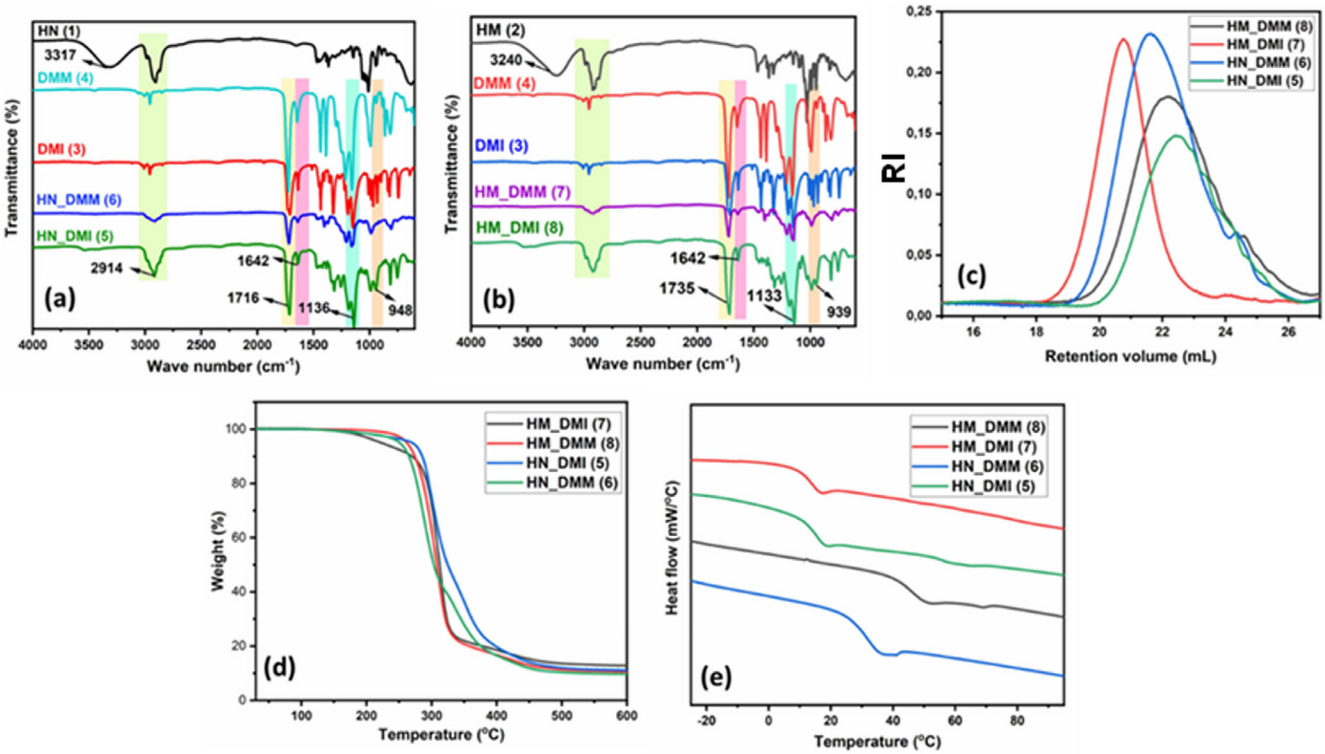

Figure 4. (a) Comparison of FTIR spectra of the polyesters (5), (6) with those of the monomers HN (1), DMI (3) and DMM (4). (b) Comparison of FTIR spectra of the polyesters (7), (8) with those of the monomer HM (2) and DMI (3) and DMM (4). (c) SEC analysis of the polyesters (5)–(8) (RI, refractive index). (d) TGA curves showing the weight loss of the polyesters (5)–(8). (e) DSC thermograms (exothermic up) from the second heating of the polyesters (5)–(8).

Table 1. Molar masses and thermal properties of the monomers (HN (1), HM (2)) and the polyesters (5)–(8)[a]

Sample	M_n SEC (g mol^{-1})	$M_{n(theo)}$ (g mol^{-1})	$Đ$	T_g (°C)	T_m (°C)	T_5 (°C)	T_d (°C)	CY (%)
HN_DMI (5)	1450	2060	1.8	15		271	295	12
HN_DMM (6)	1870	1960	2.0	30		250	287	10
HM_DMI (7)	6330	1960	1.3	13		221	315	13
HM_DMM (8)	1410	2510	2.2	45		262	310	11
HN (1)						181	244	19
HM (2)					88	170	229	20

[a]M_n and $Đ$ were measured by SEC in $CHCl_3$. $M_{n(theo)}$ was calculated from NMR. The T_g and T_m values were obtained from the second heating scan of the DSC analysis. T_5 (temperature for 5% weight loss), T_d (temperature for the maximal decomposition rate) and CY (char yield) were obtained from TGA analysis.

the snapshots. After this, each replicate formed a unique unproductive binding pose with replicate 1 flipping the ligand π-system 90° to lie flat above S165. Replicate 2 shifted to having the carbonyl hydrogen bonded to Y95 and S165 while replicate 3 dissociated completely from the catalytic serine and the western pocket, instead only staying bound by one terpene subunit in the eastern pocket with the rest of the substrate pointing out into the bulk solvent.

The aggregate result of the MD shows that LCC is capable of forming productive poses for catalysis but only occasionally, consistent with the experimental results showing release of monomer of up to 13.5% yield. Key deficiencies are the fact that the terpene subunit occupying the western pocket is not well bound, which limits the pre-organization around the catalytic triad and the oxyanion hole.

DISCUSSION

The four prepolymers reveal composition-dependent trends linking backbone structure to thermal properties and behavior. Replacing itaconate with maleate leads to rising T_g values manifested by 45 °C for HM_DMM (8) *versus* 13 °C for HM_DMI (7). For the HN-derived polyesters, the responding T_g values are 15 °C when the itaconate unit is embedded, increasing to 30 °C for maleate (Table 1). It can be noted that these glass transition temperatures are higher than typically achieved for polyester prepolymers;[77] the T_g values were even higher than for saturated aliphatic polyesters of higher molecular weight (5–17 kg mol^{-1}) generated from the same two pinene-based diols and dimethyl succinate, adipate, sebacate, respectively.[17] We ascribe this to the *cis* C=C double bond in the maleate unit, which restricts local rotation and increases packing efficiency, whereas the itaconate exo-

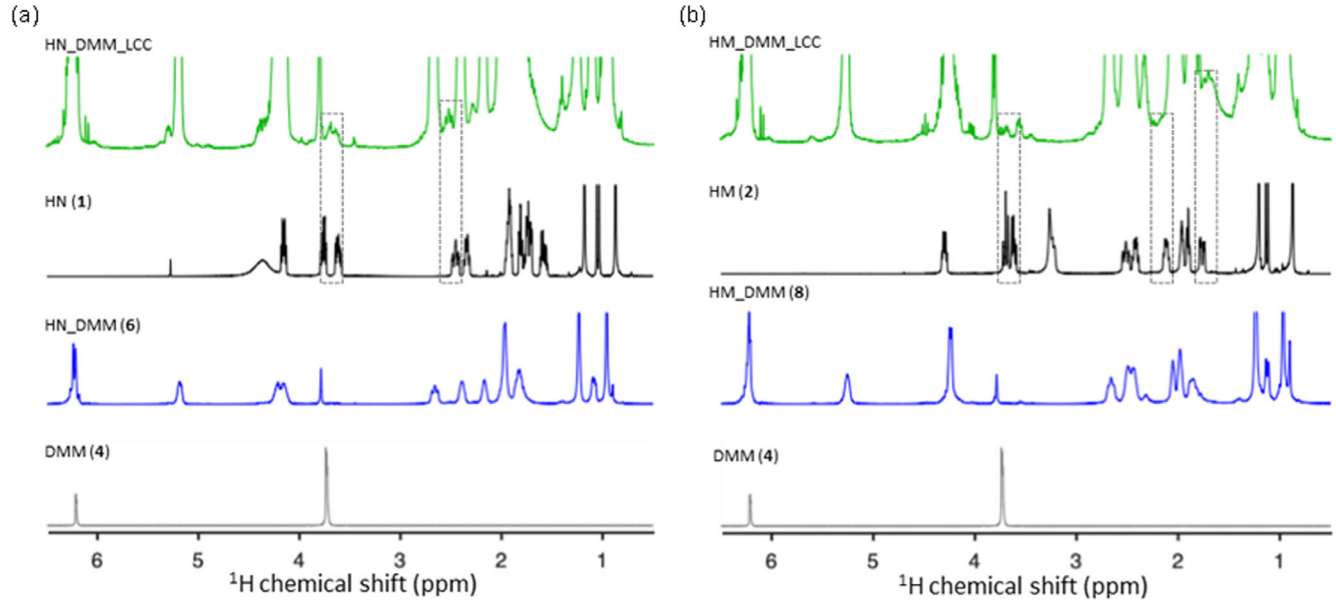

Figure 5. ^{1}H NMR spectra of polyesters before and after incubation with LCC. Polyesters including HN_DMM (a) and HM_DMM (b) were incubated with purified enzyme in the Tris–HCl buffer (pH 7.5) at 50 °C for 24 h. Released monomers from HN_DMM (a) and HM_DMM (b) were identified based on the reference spectra of the monomers HN and HM.

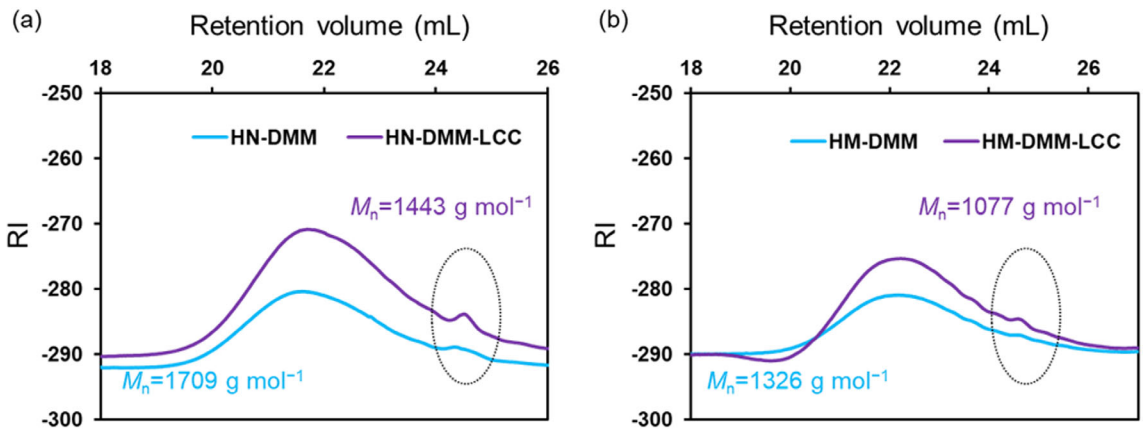

Figure 6. SEC analysis of the polyesters (a) HN_DMM (6) and (b) HM_DMM (8) before and after enzymatic incubation with LCC (RI, refractive index). The dotted black circle indicates the formation of new peaks after degradation.

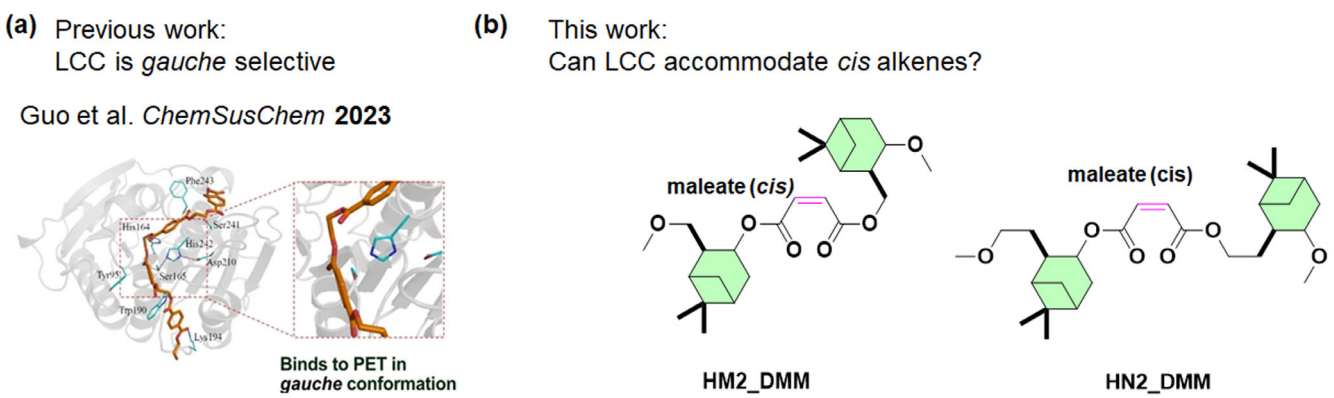

Figure 7. Exploring if conformations matter in the hydrolysis of unsaturated terpene-derived polyesters. (a) We previously showed that LCC is selective towards *gauche* PET. The figure is from Guo *et al.*[76] under CC-BY 4.0 license (b) The model substrates used to computationally represent the two polymers, HM_DMM (8) and HN_DMM (6), that were experimentally confirmed to be degraded by LCC are shown.

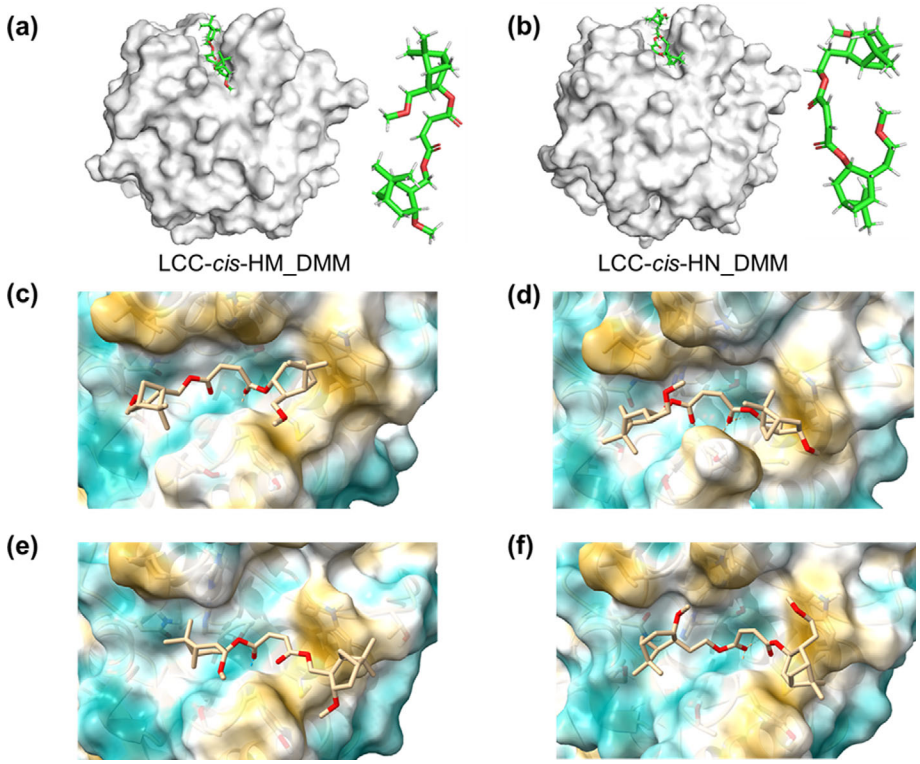

Figure 8. (a), (b) The active site location for LCC with manually posed substrate. Zoomed-in poses used for production MD after equilibration are shown in (c)–(f). (c) Manual pose of HM2_DMM. (d) Manual pose of HN2_DMM. (e) Boltz pose of HM2_DMM. (f) Boltz pose of HN2_DMM. The eastern pocket is located on the right, and the western pocket to the left, with the protein surface being colored by hydrophobicity, with lipophilic orange and polar blue.

methylene introduces greater conformational freedom in the chain. Within a given diester, the particular bicyclic diol – HN (1) *versus* HM (2) – differing in the length of the protruding chiral arm carrying the primary OH, further seems to modulate chain mobility: the by-one-methylene shorter chain attached to the bicyclic core for HM (2) is associated with the highest T_g in the series (T_g for HM_DMM (8) of 45 °C *versus* 30 °C for HN_DMM (6)) which indicates tighter segmental packing. For the itaconate-containing prepolymers, the difference in glass transition temperature is smaller between the two diols, 15 *versus* 13 °C for the HM- and HN-derived materials, which suggests a large impact from the more flexible itaconate repeating unit. All four prepolymers display good[78] thermal stability with T_5 values in the range 221–271 °C and T_d up to 315 °C, indicating that the bicyclic terpene core raises resistance to mass loss even at lower number-average molar mass in the prepolymers.

Consistent with previous studies[53,75] the LCC exhibited degradation activity toward two of the polyesters that were conformationally restricted to a *gauche*-like state (i.e. pre-organized in a NAC), namely HN_DMM (6) and HM_DMM (8). Depolymerization under mild conditions for 24 h resulted in 8% and 13.5% conversion of these polymers to the responding monomers HN (1) and HM (2), respectively. SEC analysis also confirmed the enzymatic degradation based on observation of the peak shift as well as the formation of new peaks. Moreover, the high surface area of these two powder-form polymers increases the rate of enzymatic degradation by providing more accessible sites for enzymes to bind and break down the polymer substrate.[79] This indicates that the polyesters HN_DMM (6) and HM_DMM (8) have great potential to be utilized on an industrial scale since they can be depolymerized by enzymes in a green, sustainable and cost-effective manner. In contrast, the enzyme LCC displayed no visible degradation capability against the two gel-form polyesters, including HN_DMI (5) and HM_DMI (7). This might be explained by the lower surface area and relatively higher molecular weight compared to HN_DMM (6) and HM_DMM (8).

To further understand the performance of LCC, we generated enzyme–substrate complexes using a combination of docking, metadynamics and machine learning methods. These poses were then subjected to MD, which allowed us to see that HM_DMM (8) binds better than HN_DMM (6) and that the active site of the enzyme has a polar pocket ('western pocket') which is poorly adapted to bind these substrates. The polar pocket also affected the extent of pre-organization in the enzyme as judged by the prevalence of hydrogen bonds in the oxyanion hole. This would probably limit the kinetics of the enzyme, consistent with the higher depolymerization rate for HM_DMM (8) over HN_DMM (6). However, both substrates bound in a *gauche*-like NAC, which is the preferred substrate conformation for LCC according to a conformational selection mechanism.[80]

CONCLUSION

In the present study, four new biobased unsaturated polyesters were synthesized from chiral (–)-α-pinene-derived diols (HN (1) and HM (2)) and esters of renewable dicarboxylic acids (DMI (3) and DMM (4)) under solvent-free conditions in the presence of a metal catalyst through transesterification followed by polycondensation. ^{1}H, ^{13}C NMR and FTIR confirmed an intact bicyclic α-pinene ring structure in the backbone of the unsaturated polyesters with maintained C=C bonds. SEC analysis showed that, while being prepolymers with low molecular weight, thermal

Polymer International published by John Wiley & Sons Ltd on behalf of Society of Chemical Industry.

analysis by DSC and TGA demonstrated that these polyesters have good heat resistance and elevated glass transition temperature up to 45 °C. Furthermore, two of these polymers HN_DMM (6) and HM_DMM (8) can be degraded by the LCC into their monomers HN (1) and HM (2), respectively, without any pretreatment. Based on simulations, we were able to study and visualize the geometries of the enzyme–substrate complexes, showing that substrates are pre-organized into a *gauche*-like conformation, which is the preferred substrate pose by LCC for PET[76] and saturated biobased polyesters.[75] Simulations also identified deficiencies in the binding pocket, highlighting opportunities for improving the biodegradation.

This study shows that polyesters uniting unsaturation, originating from renewable carbons, with the rigidity stemming from bulky biobased diols are attractive targets towards high-performance, circular materials with post-functionalization opportunities. Possibly, these polyesters can be crosslinked due to the presence of double bonds, which can further improve the properties of the material.

ACKNOWLEDGEMENTS

We thank Professor Minna Hakkarainen for fruitful discussions. We greatly acknowledge funding from the Swedish Research Council FORMAS (2021-02509), Carl Trygger Foundation (CTS 23:2626) and the NovoNordisk Foundation (#NNF23OC0086236). We are grateful for funding from the Swedish Energy Agency (#2023-204560). We are grateful for computational resources provided by the National Academic Infrastructure for Supercomputing in Sweden (NAISS), partially funded by the Swedish Research Council (VR) through grant agreement no. 2022-06725. We greatly acknowledge the PDC Centre for High Performance Computing at the Royal Institute of Technology and SNIC and NAISS (projects 2025/5-398 and 2025/23-373).

DATA AVAILABILITY STATEMENT

Supporting information is available with NMR spectra; additional data can be provided from the authors upon reasonable request.

CONFLICT OF INTEREST

The authors declare no competing interests.

AUTHOR CONTRIBUTIONS

R.G. conducted the synthesis and characterization of the polymers with D.B. assisting in the NMR analysis. S.W. conducted the degradation study. E.S. did the computational work while PO.S. supervised and conceptualized the study. All authors wrote the manuscript and approved the final draft for submission.

SUPPORTING INFORMATION

Supporting information may be found in the online version of this article.

REFERENCES

1 Marvel CS and Levesque CL, *J Am Chem Soc* **61**:1682–1684 (1939).
2 Geyer R, Jambeck JR and Law KL, *Sci Adv* **3**:e1700782 (2017).
3 Pottinger AS, Geyer R, Biyani N, Martinez CC, Nathan N, Morse MR *et al.*, *Science* **386**:1168–1173 (2024).
4 Inskeep GC, Taylor GG and Breitzke WC, *Ind Eng Chem* **44**:1955–1966 (1952).
5 Marvel CS and Shepherd TH, *J Org Chem* **24**:599–605 (1959).
6 Rosenboom JG, Langer R and Traverso G, *Nat Rev Mater* **7**:117–137 (2022).
7 Xu JL, Wright S, Rauert C and Thomas KV, *Nature* **639**:300–302 (2025).
8 Huang H, Hou J, Li M, Wei F, Liao Y and Xi B, *Sci Adv* **11**:eadr8243 (2025).
9 Vethaak AD and Legler J, *Science* **371**:672–674 (2021).
10 Lopez-Lorenzo X, Hueting D, Bosshard E and Syrén PO, *Faraday Discuss* **252**:387–402 (2024).
11 Tennakoon A, Wu X, Paterson AL, Patnaik S, Pei Y, LaPointe AM *et al.*, *Nat Catal* **3**:893–901 (2020).
12 Coates GW and Getzler YDYL, *Nat Rev Mater* **5**:501–516 (2020).
13 Hillmyer MA, *Science* **358**:868–870 (2017).
14 Garcia JM and Robertson ML, *Science* **358**:870–872 (2017).
15 Rahimi A and García JM, *Nat Rev Chem* **1**:0046 (2017).
16 Schwab ST, Baur M, Nelson TF and Mecking S, *Chem Rev* **124**:2327–2351 (2024).
17 Sun S and Syrén PO, *Commun Chem* **8**:272 (2025).
18 Tournier V, Duquesne S, Guillamot F, Cramail H, Taton D, Marty A *et al.*, *Chem Rev* **123**:5612–5701 (2023).
19 Wei R, Weber G, Blank LM and Bornscheuer UT, *Nat Chem Eng* **2**:110–117 (2025).
20 Wei R, Tiso T, Bertling J, O'Connor K, Blank LM and Bornscheuer UT, *Nat Catal* **3**:867–871 (2020).
21 Hermens JGH, Jensma A and Feringa BL, *Angew Chem Int Ed* **61**:e202112618 (2022).
22 Zhang X, Fevre M, Jones GO and Waymouth RM, *Chem Rev* **118**:839–885 (2018).
23 Delidovich I, Hausoul PJC, Deng L, Pfützenreuter R, Rose M and Palkovits R, *Chem Rev* **116**:1540–1599 (2016).
24 Blanksby SJ and Ellison GB, *Acc Chem Res* **36**:255–263 (2003).
25 Luo YR, *Handbook of Bond Dissociation Energies in Organic Compounds*. CRC Press, Boca Raton (2002).
26 Wang X, van Putten RJ, Tietema A, Parsons JR and Gruter GJM, *Green Chem* **26**:3698–3716 (2024).
27 Zhou P, Yuan Z, He J, Fang T, Liu B and Zhang Z, *Chem Commun* **59**:11923–11931 (2023).
28 Farhat W, Stamm A, Robert-Monpate M, Biundo A and Syrén PO, *Z Naturforsch C* **74**:90–99 (2019).
29 Zhou Z, LaPointe AM, Shaffer TD and Coates GW, *Nat Chem* **15**:856–861 (2023).
30 Häußler M, Eck M, Rothauer D and Mecking S, *Nature* **590**:423–427 (2021).
31 Wang MY, Tu YM, Zeng QQ, Li K, Xiong W, Cai Z *et al.*, *Nat Chem* **17**:1119–1128 (2025).
32 Hador R, Shuster M, Venditto V and Kol M, *Angew Chem Int Ed* **61**:e202207652 (2022).
33 Hermann A, Hill S, Metz A, Heck J, Hoffmann A, Hartmann L *et al.*, *Angew Chem Int Ed* **59**:21778–21784 (2020).
34 Lim JYC, Yuntawattana N, Beer PD and Williams CK, *Angew Chem Int Ed* **58**:6007–6011 (2019).
35 Wu Y-C, Fan H-Z, Zhang W, Wang M-Y, Cai Z and Zhu J-B, *Macromolecules* **55**:9232–9241 (2022).
36 Winnacker M, *Curr Opin Green Sustain Chem* **41**:100819 (2023).
37 Córdova T, Enríquez-Medrano FJ, Cartagena EM, Villanueva AB, Valencia L, Álvarez ENC *et al.*, *Polymers* **14**:2907 (2022).
38 Della Monica F and Kleij AW, *Polym Chem* **11**:5109–5127 (2020).
39 Thomsett MR, Moore JC, Buchard A, Stockman RA and Howdle SM, *Green Chem* **21**:149–156 (2019).
40 Stockmann PN, Pastoetter DL, Woelbing M, Falcke C, Winnacker M, Strittmatter H *et al.*, *Macromol Rapid Commun* **40**:1800903 (2019).
41 Winnacker M and Sag J, *Chem Commun* **54**:841–844 (2018).
42 Winnacker M, *Angew Chem Int Ed* **57**:14362–14371 (2018).
43 Winnacker M, Sag J, Tischner A and Rieger B, *Macromol Rapid Commun* **38**:1600787 (2017).
44 Steffen R, Irina F, Michael H and Volker S, *ChemSusChem* **10**:3574–3580 (2017).
45 Quilter HC, Hutchby M, Davidson MG and Jones MD, *Polym Chem* **8**:833–837 (2017).
46 Ojika M, Satoh K and Kamigaito M, *Angew Chem Int Ed* **56**:1789–1793 (2017).
47 Zhu Y, Romain C and Williams CK, *Nature* **540**:354–362 (2016).
48 Farhat W, Biundo A, Stamm A, Malmström E and Syrén PO, *J Appl Polym Sci* **137**:48949 (2020).

49 Stamm A, Öhlin J, Mosbech C, Olsén P, Guo B, Söderberg E *et al*., *JACS Au* **1**:1949–1960 (2021).
50 Stamm A, Tengdelius M, Schmidt B, Engström J, Syrén PO, Fogelström L *et al*., *Green Chem* **21**:2720–2731 (2019).
51 Stamm A, Biundo A, Schmidt B, Brücher J, Lundmark S, Olsén P *et al*., *Chembiochem* **20**:1664–1671 (2019).
52 Christianson DW, *Chem Rev* **117**:11570–11648 (2017).
53 Ranjani G, Subramaniyan S, Lopez-Lorenzo X, Hakkarainen M and Syrén PO, *ACS Sustain Chem Eng* **13**:6696–6705 (2025).
54 Gañán P, Barajas J, Zuluaga R, Castro C, Marín D, Tercjak A *et al*., *Polymers* **15**:2970 (2023).
55 Ates Z, Thornton PD and Heise A, *Polym Chem* **2**:309–312 (2011).
56 Lima MS, Costa CSMF, Coelho JFJ, Fonseca AC and Serra AC, *Green Chem* **20**:4880–4890 (2018).
57 Knight SC, Schaller CP, Tolman WB and Hillmyer MA, *RSC Adv* **3**:20399–20404 (2013).
58 Hauenstein O, Agarwal S and Greiner A, *Nat Commun* **7**:11862 (2016).
59 Maturi M, Spanu C, Locatelli E, Sambri L and Comes Franchini M, *Addit Manuf* **92**:104360 (2024).
60 Eberhardt J, Santos-Martins D, Tillack AF and Forli S, *J Chem Inf Model* **61**:3891–3898 (2021).
61 Du L, Geng C, Zeng Q, Huang T, Tang J, Chu Y *et al*., *Brief Bioinform* **24**: bbad047 (2023).
62 Eastman P, Galvelis R, Peláez RP, Abreu CRA, Farr SE, Gallicchio E *et al*., *J Phys Chem B* **128**:109–116 (2024).
63 Maier JA, Martinez C, Kasavajhala K, Wickstrom L, Hauser KE and Simmerling C, *J Chem Theory Comput* **11**:3696–3713 (2015).
64 Boothroyd S, Behara PK, Madin OC, Hahn DF, Jang H *et al*., *J Chem Theory Comput* **19**:3251–3265 (2023).
65 Wang LP, Martinez TJ and Pande VS, *J Phys Chem Lett* **5**:1885–1891 (2014).
66 Barducci A, Bussi G and Parrinello M, *Phys Rev Lett* **100**:020603 (2008).
67 Gowers RJ, Linke M, Barnoud J, Reddy TJE, Melo MN *et al*., A Python package for the rapid analysis of molecular dynamics simulations. *Proc 15th Python in Science Conf*, SciPy, Austin, TX, USA, pp. 102–109 (2016).
68 Michaud-Agrawal N, Denning EJ, Woolf TB and Beckstein O, *J Comput Chem* **32**:2319–2327 (2011).
69 Tiberti M, Papaleo E, Bengtsen T, Boomsma W and Lindorff-Larsen K, *PLoS Comput Biol* **11**:e1004415 (2015).
70 Bouysset C and Fiorucci S, *J Chem* **13**:72 (2021).
71 Meng EC, Goddard TD, Pettersen EF, Couch GS, Pearson ZJ, Morris JH *et al*., *Protein Sci* **33**:e4792 (2024).
72 Zeng W, Li X, Yang Y, Min J, Huang JW, Liu W *et al*., *ACS Catal* **12**:3033–3040 (2022).
73 Passaro S, Corso G, Wohlwend J, Reveiz M, Thaler S et al., *bioRxiv 2025* 2025.06.14.659707 (2025).
74 Abid U, Sun G, Soong YHV, Williams A, Chang AC, Ayafor C *et al*., *Biochem Eng J* **199**:109074 (2023).
75 Lopez-Lorenzo X, Ranjani G and Syrén PO, *Chembiochem* **26**: e202400456 (2025).
76 Guo B, Lopez-Lorenzo X, Fang Y, Bäckström E, Capezza AJ, Vanga SR *et al*., *ChemSusChem* **16**:e202300742 (2023).
77 Ramis X and Salla JM, *J Polym Sci B* **35**:371–388 (1997).
78 Chu F, Hu Y, Hu W, Song L and Hu Y, *Compos Part B Eng* **294**:112171 (2025).
79 Suresh V, Shams R, Dash KK, Shaikh AM and Béla K, *J Agric Food Res* **20**: 101788 (2025).
80 Guo B, Vanga SR, Lopez-Lorenzo X, Saenz-Mendez P, Ericsson SR, Fang Y *et al*., *ACS Catal* **12**:3397–3409 (2022).